CHALMERS
UNIVERSITY OF TECHNOLOGY

Error-bounded Reference Tracking Mpc for Machines with Structural Flexibility

Citation for the original published paper (version of record):
Yuan, M. (2020). Error-bounded Reference Tracking Mpc for Machines with Structural Flexibility. IEEE Transactions on Industrial Electronics, 67(10): 8143-8154.
http://dx.doi.org/10.1109/TIE.2019.2949521

(article starts on next page)

Error-Bounded Reference Tracking MPC for Machines With Structural Flexibility

Meng Yuan, *Student Member, IEEE*, Chris Manzie, *Senior Member, IEEE*, Malcolm Good, *Member, IEEE*, Iman Shames, *Member, IEEE*, Lu Gan, Farzad Keynejad, and Troy Robinette

***Abstract*—For industrial contouring and machining applications such as laser cutting, it is desirable to be able to bound errors without unduly compromising machine throughput. Traditional control architectures in machining are unable to explicitly bound tracking errors, and therefore, conservative operation is required to ensure satisfactory performance of the overall system. This is particularly relevant in contouring applications when the end effector is connected to the drive via a flexible link, and no direct feedback measurement about the end-effector position is available. In this article, a model predictive approach is proposed, which guarantees that a desired level of tracking error is met for the case where the structure is flexible and the end-effector position is estimated. To achieve this, a robust control invariant set is estimated using a computationally tractable algorithm and incorporated into the problem formulation. The applicability of the proposed approach is successfully demonstrated via simulation and experiments conducted on a commercial single axis system.**

***Index Terms*—Flexible structures, model predictive control (MPC), motion control.**

I. Introduction

In THE field of industrial precision motion control, many applications require the manipulated unit to track a time-varying reference or a given path as closely as possible. Tracking error plays an important role in measuring the control performance. In multiaxial application, the contouring error can be ultimately reduced by enhancing the tracking performance of each axis individually [1].

Manuscript received March 5, 2019; revised June 3, 2019, August 8, 2019, and September 19, 2019; accepted October 13, 2019. Date of publication October 30, 2019; date of current version June 3, 2020. This work was supported by the University of Melbourne through the Melbourne International Fee Remission Scholarship (MIFRS) and Melbourne International Research Scholarship (MIRS). *(Corresponding author: Meng Yuan.)*

M. Yuan and M. Good are with the Department of Mechanical Engineering, The University of Melbourne, Parkville, VIC 3010, Australia (e-mail: yuanm3@student.unimelb.edu.au; mcgood@unimelb.edu.au).

C. Manzie and I. Shames are with the Department of Electrical and Electronic Engineering, The University of Melbourne, Parkville, VIC 3010, Australia (e-mail: mcgood@unimelb.edu.au; iman.shames@unimelb.edu.au).

L. Gan, F. Keynejad, and T. Robinette are with ANCA Motion, Bayswater North, VIC 3153, Australia (e-mail: lu.gan@ancamotion.com; farzad.keynejad@ancamotion.com; troy.robinette@ancamotion.com).

Color versions of one or more of the figures in this article are available online at http://ieeexplore.ieee.org.

Digital Object Identifier 10.1109/TIE.2019.2949521

Traditionally, the manipulators are built with high stiffness and are assumed to be as rigid in models used for controller synthesis. Greater rigidity results in more weight. Consequently, larger and more costly motors are required to perform a given operation in a timely fashion [2]. Alternatively, using lighter (but more flexible) manipulators promises faster movements and more efficient utilization of energy. However, the flexibility of the lightweight structure can lead to system vibration, which degrades the trajectory tracking performance [3] and may even lead to system instability [4]. This problem can be found in gantry machines [5], machine tools [6], crane moving systems [7], and servo drive systems [8].

To improve the trajectory-tracking performance of systems with flexible linkages, a range of control methods have been proposed in the industrial motion control field. This includes position command prefiltering [9], notch filter inserting [10], proportional-integral (PI) control [11], and PI control with additional feedback loops [12]. The inclusion of filters is common in industrial applications; however, this usually reduces the position tracking bandwidth relative to potential control augmentation with end-effector feedback. Furthermore, although it is easy to implement cascaded PI-based control laws, this reactive method requires a degree of positioning error to enact control effort and demands a large commissioning effort in practice [13].

Typically, controllers using an explicit plant model consider only the first few vibrational modes of the system, and it is common to see only the first mode of vibration considered during controller design. The system is usually simplified as a two-mass system [3], [8]. In [8], cascaded controller with additional feedback was used to reduce the vibration of end effector/load. In [3], pole placement and trajectory planning are combined to achieve asymptotic tracking. However, constraints are not explicitly considered in these approaches. System constraints, whether influenced by physical limitations or restricting the operation of the system to a desirable envelope, are of great importance for ensuring continued robust operation. Model predictive control (MPC) can take constraints explicitly into controller design formulation and consequently, becomes a potentially attractive approach for solving these problems.

In [4] and [14], MPC-based speed and position tracking are designed for two-mass disturbance-free system and experimental results illustrate the tracking performance. However, achieving asymptotically offset-free tracking for disturbance-free system is not enough. For applications such as laser cutting,

the workpiece is qualified only if the contouring error is within a desired tolerance or the tracking error of each axis is in a given error bound during the whole process. It has to be noticed that without small enough tracking error bounds on all axes, the contouring error cannot be guaranteed to be within the desired range as shown in [15]. In these cases, the desired tracking error bound can be regarded as a performance constraint of the closed-loop system.

In [16], an error-bounded tracking controller is designed for a linear time invariant (LTI) system subjected to state and input constraints. A robust control invariant (RCI) set is utilized to ensure that the state, input, and performance constraints can be guaranteed in the application of MPC. The authors offer an algorithm for calculating a polyhedral RCI set and design an MPC to guarantee that the system constraints and tracking error bound are satisfied during operation, and demonstrate the closed-loop system using simulations. However, considering that the RCI set may not be finitely determined for system with state disturbance [17], it is nontrivial to calculate the RCI set for a practical system that includes state disturbance.

Although the problem of calculating an RCI set has been studied extensively [17]–[19], there are few papers that consider input and state constraints in the system, as well as the impact of disturbances on them. In [19], the authors proposed an algorithm to compute the RCI for a system with state and input-dependent disturbance. However, the calculated set is generally nonconvex even if the constraint sets of state, input, and disturbance are polyhedral, which makes the calculated set nonapplicable for practical controller design. Although [16] and [20] proposed a way to compute a convex and polyhedral RCI set for systems with state-dependent disturbance, it is still hard to check the existence of the RCI set for a given problem, as the proposed algorithm may return an empty RCI set when the set is not finitely determined and the maximum number of computation iterations is reached—leading to an iterative trial-and-error situation where either the disturbance set is required to decrease or the number of iteration needs to be increased.

In this article, an error-bounded tracking controller formulation for a system with structural flexibility and state-dependent disturbance is proposed. Different from [16], the proposed RCI calculation algorithm is guaranteed to terminate in a finite number of steps. The existence of the calculated RCI set indicates that the error bound can be guaranteed for particular classes of reference and system, with consideration of state and input constraints. For systems with structural flexibility, the work of [21] is extended by using an observer integrated error-bounded control architecture and the approach is validated on an industrial test bench with 1-kHz sampling rate.

The rest of this article is organized as follows. In Section II, the system and reference models are introduced. Section III describes the design of an observer for the case that end-effector information is not available, and introduces the proposed RCI set calculation algorithm and the MPC methodology. Section IV demonstrates the performance of the proposed controller, and comparison with a conventional industrial tracking controller is given. The conclusion is given in Section V.

Notation: $\mathbb{R}$, $\mathbb{R}_+$ and $\mathbb{Z}$, $\mathbb{Z}_+$, $\mathbb{Z}_{0+}$ are the sets of real, positive real and integer, positive integer, nonnegative integer numbers. An identity matrix of size n is denoted by I_n and an $m \times n$ zero matrix is denoted by $0_{m,n}$. Consider $a \in \mathbb{R}^{n_a}, b \in \mathbb{R}^{n_b}$, then $(a, b) \triangleq [a^T, b^T]^T \in \mathbb{R}^{n_a+n_b}$ represents the stacked vector. The set $\mathbb{B}^n(\rho)$ is a closed ball in $\mathbb{R}^n$ with respect to the infinity norm with ρ radius. For two sets $\mathcal{X}$ and $\mathcal{Y}$, $\mathcal{X} - \mathcal{Y}$ is the Minkowski difference. The vector $x(k)$ is the value at sampling instant k, the time $T_s \cdot k$, where T_s is the sampling period, and x^+ stands for the value of x at the next time instant. Vector $x_{i|k}$ represents the predicted value of x at the time sample $k + i$ based on the data at sample k.

II. System Description and Problem Statement

As closed-loop performance is most significantly influenced by the fundamental mechanical vibration frequency [22], the two-degree-of-freedom model with additional lumped disturbance is widely used to represent systems with flexibility and nonlinear disturbances, with the following representation of the mechanical system dynamics:

$$\begin{aligned} x_m^+ &= x_m + T_s v_m \\ v_m^+ &= v_m + \frac{T_s}{M_m}\left(k_t u - k_s\left(x_m - x_e\right) - c_s\left(v_m - v_e\right) - F_{d1}\right) \\ x_e^+ &= x_e + T_s v_e \\ v_e^+ &= v_e + \frac{T_s}{M_e}\left(k_s\left(x_m - x_e\right) + c_s\left(v_m - v_e\right) - F_{d2}\right) \end{aligned} \tag{1}$$

where M_m, M_e are the nominal value of the motor and end-effector masses; x_m and x_e are the position of the motor and end effector separated by the flexible link; v_m and v_e are the velocity of the motor and end effector, respectively; u is the current to the drive system; k_t is the nominal value of the motor force constant; k_s and c_s are the spring constant and internal damping coefficient of the flexible link; F_{d1} and F_{d2} stand for the lumped bounded disturbances on the motor velocity and end-effector velocity dynamics, respectively, which may include plant model mismatch arising from un-modeled dynamics or imperfect model parameters, as well as noise effects.

The mechanical system dynamics (1) can be written in state-space form with the viscous friction explicitly considered in the system matrices

$$\xi^+ = A_d\xi + B_d u + E_d F_d \quad y_d = C_d\xi \tag{2}$$

where the state vector is $\xi \triangleq (x_m, v_m, x_e, v_e)$ and y_d is the measured output; $F_d \triangleq (\delta, F_{d2})$ is the disturbance vector with $\delta \triangleq F_{d1} - b_v v_m$ and b_v is the viscous friction coefficient. The specific matrices of the LTI model (2) are given as

$$A_d = \begin{bmatrix} 1 & T_s & 0 & 0 \\ -\frac{T_s k_s}{M_m} & \frac{M_m - T_s(c_s + b_v)}{M_m} & \frac{T_s k_s}{M_m} & \frac{T_s c_s}{M_m} \\ 0 & 0 & 1 & T_s \\ \frac{T_s k_s}{M_e} & \frac{T_s c_s}{M_e} & -\frac{T_s k_s}{M_e} & \frac{M_e - T_s c_s}{M_e} \end{bmatrix}$$

$$B_d = \begin{bmatrix} 0 \\ \frac{T_s k_t}{M_m} \\ 0 \\ 0 \end{bmatrix}, \quad E_d = \begin{bmatrix} 0 & 0 \\ -\frac{T_s}{M_m} & 0 \\ 0 & 0 \\ 0 & -\frac{T_s}{M_e} \end{bmatrix}. \tag{3}$$

The state and input are assumed to belong to prescribed convex sets, and the external lumped disturbances are unknown and are assumed to be in closed and bounded sets, i.e.,

$$\xi \in \mathcal{X} \quad u \in \mathcal{U} \quad \delta \in \Delta \quad F_{d2} \in \mathcal{F}. \tag{4}$$

Here, (A_d, B_d) is controllable. We assume (C_d, A_d) is observable and C_d has full row rank. Furthermore, to ensure error-bounded tracking, it is necessary to impose constraints on the reference that can be tracked. With this in mind, the reference is assumed to be generated by an external LTI system

$$r^+ = A_r r + B_r u_r \quad y_r = C_r r \tag{5}$$

where $r \in \mathbb{R}^{n_r}$, $u_r \in \mathbb{R}^{m_r}$, $y_r \in \mathbb{R}$ are the state, input, and output of the reference model, subject to the constraints

$$r \in \mathcal{X}^r \quad u_r \in \mathcal{U}^r. \tag{6}$$

Moreover, it is considered that the reference is generated offline, and as such, a sufficient amount of preview of the reference trajectory (denoted N sampling instants) is available at each time step.

Ultimately, it is desirable to ensure that the tracking error between the end effector and the reference is bounded by some constant value ϵ to ensure the tolerance of the machined part. This tracking error requirement can be represented as

$$\|y_r(k) - x_e(k)\|_\infty \leq \epsilon. \tag{7}$$

The complete problem of interest here is formalized as follows.

Problem 1: Consider system (2) subject to (4) with reference generated by (5) satisfying (6). Given a desired tolerance $\epsilon \in \mathbb{R}_+$ and initial conditions satisfying (4) and (7), design a feedback control law $u(k) = \kappa(\cdot)$, such that the closed-loop system satisfies (7) for all $k \in \mathbb{Z}_{0+}$.

III. Proposed Control Architecture

Due to the presence of constraints, MPC is a good candidate to solve Problem 1. This typically involves solving an open-loop optimization problem at each time step subject to constraints that reflect the system dynamics and operational constraints, without sacrificing feasibility of the optimization problem at future time intervals.

In order to guarantee recursive feasibility of the MPC problem, one approach is to ensure that the system and reference states stay inside an RCI set [16]. For most industrial systems, it is hard or impossible to measure the position and velocity of the end effector. We seek to guarantee the error between reference and estimated position in a tighter tolerance in order to bound the true end-effector tracking error within the desired tolerance. An augmented system that incorporates the dynamics of estimated states is thus required for controller design.

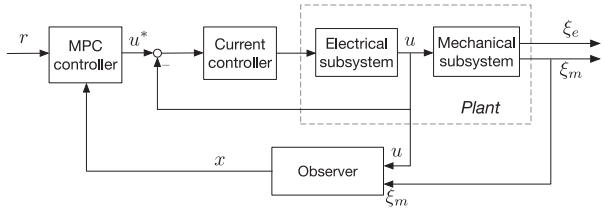

Fig. 1. Proposed control structure for error-bounded tracking.

In the subsequent subsections, the observer design and augmented system dynamics are described. For systems where the RCI set may not be finitely determined, the offline RCI set estimation approach proposed in this article is presented in detail, leading to the formulation of the MPC problem used to address Problem 1. The entire closed-loop structure is illustrated in Fig. 1. Since the time scale of the electrical subsystem is much faster than the mechanical subsystem, the design of the current controller is not considered in this article.

A. Estimation of the End-Effector States

In general, the value of C_d depends on the measurable states of the system. In this article, only the position and velocity of the motor are measurable. Thus, the explicit expression of C_d is

$$C_d = \begin{bmatrix} 1 & 0 & 0 & 0 \\ 0 & 1 & 0 & 0 \end{bmatrix}.$$

The mechanical system dynamics (2) can be written in partitioned matrix form based on measured and unmeasured states as

$$\xi^+ = \left[\begin{array}{c|c} A_{11} & A_{12} \\ \hline A_{21} & A_{22} \end{array}\right] \begin{bmatrix} \xi_m \\ \xi_e \end{bmatrix} + \begin{bmatrix} B_1 \\ B_2 \end{bmatrix} u + \left[\begin{array}{c|c} E_1 & 0_{2,1} \\ \hline 0_{2,1} & E_2 \end{array}\right] \begin{bmatrix} \delta \\ F_{d2} \end{bmatrix} \tag{8}$$

where $\xi_m \triangleq (x_m, v_m)$, $\xi_e \triangleq (x_e, v_e)$. Let $\hat{\xi}_e \triangleq (\hat{x}_e, \hat{v}_e)$, where $\hat{x}_e$ and $\hat{v}_e$ are the estimated position and velocity of end effector, respectively. A Luenberger observer with observer gain L_r for the unmeasured state can be formulated as

$$\hat{\xi}_e^+ = A_{22}\hat{\xi}_e + A_{21}\xi_m + B_2 u + L_r(\xi_m^+ - A_{11}\xi_m - B_1 u - A_{12}\hat{\xi}_e). \tag{9}$$

To avoid causality issues in calculating ξ_m^+, an auxiliary variable $z = \hat{\xi}_e - L_r\xi_m$ can be introduced with dynamics as follows:

$$\begin{aligned} z^+ &= \hat{\xi}_e^+ - L_r\xi_m^+ \\ &= (A_{22} - L_rA_{12})\, z + (B_2 - L_rB_1)\, u \\ &\quad + ((A_{22} - L_rA_{12})\, L_r + A_{21} - L_rA_{11})\, \xi_m. \end{aligned} \tag{10}$$

The reduced-order estimation error can be defined as $\tilde{\xi}_e = \xi_e - \hat{\xi}_e$. The error dynamics are given by

$$\begin{aligned} \tilde{\xi}_e^+ &= \xi_e^+ - \hat{\xi}_e^+ \\ &= (A_{22} - L_rA_{12})\, \tilde{\xi}_e - L_rE_1\delta + E_2F_{d2}. \end{aligned} \tag{11}$$

The measured states ξ_m are then combined with the auxiliary variable to form an augmented state vector $x \triangleq (\xi_m, z)$. Denote the output of augmented system as $y \triangleq (\xi_m, \hat{\xi}_e)$, and the dynamics of this augmented system is given as follows:

$$\begin{aligned} x^+ &= \begin{bmatrix} A_{11}+A_{12}L_r & A_{12} \\ \Theta L_r + A_{21} - L_r A_{11} & A_{22} - L_r A_{12} \end{bmatrix} x \\ &\quad + \begin{bmatrix} B_1 \\ B_2 - L_r B_1 \end{bmatrix} u + \begin{bmatrix} I_2 \\ 0_{2,2} \end{bmatrix} \left(E_1 \delta + A_{12} \tilde{\xi}_e \right) \\ &:= Ax + Bu + Ew \\ y &= Cx \end{aligned} \tag{12}$$

where the matrix C can be inferred from the state x and output y; $\Theta \triangleq (A_{22} - L_r A_{12})$; $w \triangleq E_1\delta + A_{12}\tilde{\xi}_e$ is considered as a combined disturbance. This lumped disturbance is assumed within closed and bounded sets as $w \in \mathcal{W}$, where the range of set $\mathcal{W}$ can be identified. The observer gain L_r should be chosen to ensure the eigenvalues of Θ are inside the unit circle when designing the observer. In this article, the gain of the partial state observer is chosen (after some tuning) to be

$$L_r = \begin{bmatrix} 0 & 0.001 \\ 0 & 0.001 \end{bmatrix}.$$

From (11), it follows that given a positive constant ϵ_o, there exists a positive pair of sets (Ω, Γ) such that for all $||\tilde{\xi}_e(0)||_\infty \in \Omega$ and $||(\delta(k), F_{d2}(k))||_\infty \in \Gamma \ \forall k \in \mathbb{Z}_{0+}$, the estimator maintains a bounded estimation error performance, i.e.,

$$\|x_e(k) - \hat{x}_e(k)\|_\infty \leq \epsilon_o \ \forall k \in \mathbb{Z}_{0+}. \tag{13}$$

To ensure this infinity bound can be satisfied in practice, it is necessary that the system must be started from a limited range of initial conditions—for example, the end effector is at rest and on the desired trajectory initially.

The control problem then becomes ensuring that for a given desired tolerance ϵ, the difference between the reference position and the estimated position of the end effector is bounded by $\|y_r(k) - \hat{x}_e(k)\|_\infty \leq \epsilon_c = \epsilon - \epsilon_o$.

Remark 1: In practice, the upper bound of the estimation error ϵ_o is identified first. Then, a desired tracking error bound ϵ is chosen to ensure $\epsilon_o \leq \epsilon$. If the estimation error is within an error bound $\|\hat{x}_e - x_e\|_\infty \leq \epsilon_o$ and the designed controller can guarantee $\|y_r - \hat{x}_e\|_\infty \leq \epsilon - \epsilon_o$, we can ensure that the end-effector tracking error is always within the desired error bound $\|y_r - x_e\|_\infty \leq \epsilon$. This inequality is based on the triangular inequality

$$\|y_r - x_e\|_\infty \leq \|y_r - \hat{x}_e\|_\infty + \|\hat{x}_e - x_e\|_\infty.$$

B. Estimation of the Maximal Robust Control Invariant Set

The following three definitions are presented for completeness in the most general setting.

Definition 1: (RCI and maximal RCI sets) Consider the system $x^+ = Ax + Bu + Ew$, where $x \in \mathcal{X} \subseteq \mathbb{R}^n, u \in \mathcal{U} \subseteq \mathbb{R}^m$, and $w \in \mathcal{W} \subseteq \mathbb{R}^d$ are the state, input, and disturbance vectors. The set $\mathcal{R} \subseteq \mathcal{X}$ is an RCI set if

$$x(k) \in \mathcal{R}, \exists_{u \in \mathcal{U}}, Ax + Bu + Ew \in \mathcal{R} \quad \forall w \in \mathcal{W} \ \forall k \in \mathbb{Z}_{0+}.$$

Furthermore, the set $\mathcal{R}$ is called a control invariant (CI) set if $w = 0$; the set $\mathcal{R}_\infty$ is the maximal RCI set if any $\mathcal{R} \subseteq \mathcal{R}_\infty$.

Definition 2: (Robust admissible input set) The robust admissible input set of $\mathcal{R}$ is

$$\Theta^u(x) = \{u \in \mathcal{U} | Ax + Bu + Ew \in \mathcal{R}, \quad \forall w \in \mathcal{W}\}.$$

Definition 3: (Preset) The preset represents the set of states that can be robustly steered to a given set $\mathcal{Y} \in \mathbb{R}^n$ in one step under any possible disturbance $w \in \mathcal{W}$, and can be computed as

$$D(\mathcal{Y}, \mathcal{W}) \triangleq \{x \in \mathbb{R}^n | \exists_{u \in \mathcal{U}}, Ax + Bu + Ew \in \mathcal{Y} \ \forall w \in \mathcal{W}\}. \tag{14}$$

Denote the maximal control invariant set of the reference by $\mathcal{R}^r_\infty$. We assume the reference is generated offline and stays within the set, i.e., $r(k) \in \mathcal{R}^r_\infty \ \forall k \in \mathbb{Z}_{0+}$ by selecting $u_r(k) \in \Theta^{u_r}(r(k)) \subseteq \mathcal{U}^r$, where $\Theta^{u_r}(r_k)$ is the robust admissible input set of the reference system. This guarantees that the constraints in (6) are satisfied.

Having ensured the invariance of the reference, we now shift attention to ensuring $\|y_r - \hat{x}_e\|_\infty \leq \epsilon_c$. We begin by defining an initial set of the system and admissible reference states

$$\mathcal{S}^{x,r} = \{(x, r) | Cx \in \mathcal{X}, r \in \mathcal{R}^r_\infty, \|y_r - \hat{x}_e\|_\infty \leq \epsilon_c\}.$$

At any time $k \in \mathbb{Z}_{0+}$, if $(x(k), r(k)) \in \mathcal{S}^{x,r}$, the system constraints are satisfied and the tracking error requirement is guaranteed. Consequently, the controller synthesis problem must ensure $(x(k+1), r(k+1)) \in \mathcal{S}^{x,r}$ for every admissible $r(k+1) \subseteq \mathcal{R}^r_\infty$. This requires an RCI set of the augmented system $\mathcal{R}^{x,r} \subseteq \mathcal{S}^{x,r}$, i.e.,

$$\begin{aligned} (x, r) \in \mathcal{R}^{x,r}, \exists_{u \in \mathcal{U}}, (Ax + Bu + Ew, A_r r + B_r u_r) \in \mathcal{R}^{x,r} \\ \forall (w, u_r) \in (\mathcal{W}, \Theta^{u_r}(r)). \end{aligned} \tag{15}$$

One method of computing this RCI set $\mathcal{R}^{x,r}$ involves the iteration $\mathcal{R}_{i+1} = D(\mathcal{R}_i, (\mathcal{W} \times \Theta^{u_r}(r))) \cap \mathcal{R}_i$, where $\mathcal{R}_0 = \mathcal{S}^{x,r}$, until $\mathcal{R}_i = \mathcal{R}_{i+1}$ and $\mathcal{R}^{x,r} = \mathcal{R}^{x,r}_\infty = \mathcal{R}_i$. If this property can be satisfied, the maximal RCI set $\mathcal{R}^{x,r}_\infty$ is called finitely determined [17].

In [23], the maximal RCI set is computed as a union of polyhedra, which is nonconvex and leads to the complexity in terms of the convex elements growing exponentially with the number of iterations. In [16], an algorithm is proposed to compute a convex RCI set, but relies on the computation of the preset (14). The stopping criterion for the algorithm relies on either reaching a maximum number of iterations (i.e., no solution found) or the maximal set estimate being equal at successive iterations. This latter condition may be numerically difficult to be satisfied, and consequently, we propose a modification here based on an *estimate* of the preset using an inner approximation [17]

$$\begin{aligned} \hat{D}(\mathcal{Y}, \rho) = \{x \in \mathbb{R}^n | \exists_{u \in \mathcal{U}}, Ax + Bu + Ew \subseteq \mathcal{Y} - \mathbb{B}^n(\rho) \\ \forall w \in \mathcal{W}\}. \end{aligned} \tag{16}$$

Algorithm 1: RCI Set Computation.

Initialization:
$i \leftarrow 0$, $\mathcal{R}_0 \leftarrow \mathcal{R}_s \cap \bar{\mathcal{R}}_0$, where
$\mathcal{R}_s \leftarrow (\mathbb{R}^n \times \mathcal{R}^r_\infty)$,
$\bar{\mathcal{R}}_0 \leftarrow \{(x,r) \in \mathbb{R}^{n+n_r} | \, Cx \in \mathcal{X}, \|y_r - \hat{x}_e\|_\infty \leq \epsilon_c\}$.
Iteration:
$\mathcal{R}_{i+1} \leftarrow \mathcal{R}_s \cap \bar{\mathcal{R}}_{i+1}$, where
$\bar{\mathcal{R}}_{i+1} \leftarrow \hat{D}(\bar{\mathcal{R}}_i, \rho) \cap \bar{\mathcal{R}}_i$,

$$\hat{D}\left(\bar{\mathcal{R}}_i, \rho\right) \leftarrow \big\{(x,r) \in \mathbb{R}^{n+n_r} | \, \exists_{u \in \mathcal{U}}, \; (Ax + Bu + Ew, A_r r + B_r u_r) \in \bar{\mathcal{R}}_i - \mathbb{B}^{n+n_r}(\rho), \; \forall (w \times u_r) \in (\mathcal{W} \times \mathcal{U}^r)\big\}. \tag{17}$$

if $\mathcal{R}_i - \mathbb{B}^{n+n_r}(\rho) \subseteq \mathcal{R}_{i+1}$ **then**
  return $\mathcal{R}^{x,r} \leftarrow \mathcal{R}_{i+1}$
else
  $i \leftarrow i+1$
  go to 4
end if

The parameter ρ in this equation is a tuning parameter that can be used to influence the conservativeness of the estimate; i.e., a larger ρ leads to a more conservative estimate of the preset [17]. The modified algorithm for estimating $\mathcal{R}^{x,r}$ is now given as Algorithm 1.

The inclusion of the ρ-radius ball in the stopping criterion ensures that the computed $\mathcal{R}_{i+1}$ is an RCI set. The key difference in the proposed algorithm here relates to the inclusion of the estimate, which enables a finite number of iterations to be employed. This is proven in the following theorem.

Theorem 1: Given a prescribed tracking error bound ϵ_c and a closed ball with radius ρ, Algorithm 1 terminates in finite steps. If the computed set $\mathcal{R}_{i+1} \neq \emptyset$, then $\mathcal{R}^{x,r} = \mathcal{R}_{i+1} \subseteq \mathcal{R}^{x,r}_\infty$ is a polyhedral RCI set for (5) and (12) subjected to input constraint, and robust to $w \in \mathcal{W}$ and $u_r \in \Theta^{u_r}(r)$.

Proof: The proof includes two parts—showing the finite termination of the computing RCI set and the calculated $\mathcal{R}^{x,r}$ is an RCI set. First, the finite termination of the algorithm is shown. If $\mathcal{R}_i = \emptyset$, specifically $\mathcal{R}_s \cap \bar{\mathcal{R}}_i = \emptyset$, it implies $\mathcal{R}_{i+1} = \mathcal{R}_s \cap \hat{D}(\bar{R}_i, \rho) \cap \bar{\mathcal{R}}_i = \emptyset$. Since $\emptyset \subseteq \emptyset$, for $i \in \mathbb{Z}_{0+}$ with $\mathcal{R}_i = \emptyset$ stop criterion holds.

If $\mathcal{R}_i \neq \emptyset$ for $i \in \mathbb{Z}_{0+}$, we assume maximal RCI set $\mathcal{R}^{x,r}_\infty$ exists. As in [17], we have $\mathcal{R}^{x,r}_\infty = \lim_{i \to \infty} \mathcal{R}_i$ and there exists $j \in \mathbb{Z}_{0+}$ such that $\mathcal{R}_i - \mathbb{B}^{n+n_r}(\rho) \subseteq \mathcal{R}^{x,r}_\infty \; \forall i \geq j$. Thus, $\mathcal{R}_i - \mathbb{B}^{n+n_r}(\rho) \subseteq \mathcal{R}_{i+1}$ holds since $\mathcal{R}^{x,r}_\infty \subseteq \mathcal{R}_{i+1} \; \forall i \in \mathbb{Z}_{0+}$.

The proof that $\mathcal{R}_{i+1}$ is an RCI set is given as follows. Suppose $(x,r) \in \mathcal{R}_{i+1} = \mathcal{R}_s \cap \hat{D}(\bar{\mathcal{R}}_i, \rho) \cap \bar{\mathcal{R}}_i$, $\mathcal{R}_s \cap \hat{D}(\bar{\mathcal{R}}_i, \rho)$ can be rewritten as

$$\begin{aligned} &\mathcal{R}_s \cap \hat{D}\left(\bar{\mathcal{R}}_i, \rho\right) \\ &= \{(x,r) | \, r \in \mathcal{R}^r_\infty, \exists_{u \in \mathcal{U}}, \\ &\quad (Ax + Bu + Ew, A_r r + B_r u_r) \in \bar{\mathcal{R}}_i - \mathbb{B}^{n+n_r}(\rho) \\ &\quad \forall (w \times u_r) \in (\mathcal{W} \times \mathcal{U}^r)\}. \end{aligned} \tag{18}$$

Since the order of projection and intersection can be inverted considering that $\mathcal{R}_s$ is independent of the projection variable u and $\mathcal{R}_i = \mathcal{R}_s \cap \bar{\mathcal{R}}_i$, (18) can be represented as

$$\begin{aligned} &\mathcal{R}_s \cap \hat{D}\left(\bar{\mathcal{R}}_i, \rho\right) \\ &= \big\{(x,r) | \, \exists_{u_r \in \Theta^{u_r}(r)}, A_r r + B_r u_r \in \mathcal{R}^r_\infty, \\ &\quad \exists_{u \in \mathcal{U}}, (Ax + Bu + Ew, A_r r + B_r u_r) \in \mathcal{R}_i - \mathbb{B}^{n+n_r}(\rho) \\ &\quad \forall (w \times u_r) \in (\mathcal{W} \times \mathcal{U}^r)\big\}. \end{aligned} \tag{19}$$

Because $\mathcal{R}_i - \mathbb{B}^{n+n_r}(\rho) \subseteq \mathcal{R}_{i+1}$ according to the stop criterion, (19) means that there exists $u \in \mathcal{U}$ such that $(Ax + Bu + Ew, A_r r + B_r u_r) \in \mathcal{R}_i - \mathbb{B}^{n+n_r}(\rho) \subseteq \mathcal{R}_{i+1}$. This implies $(Ax + Bu + Ew, A_r r + B_r u_r) \in \mathcal{R}_{i+1}$, which shows R_{i+1} is an RCI set according to Definition 1.

The property $\mathcal{R}^{x,r} \subseteq \mathcal{R}^{x,r}_\infty$ follows from the proof in [16], so the details are omitted here. The RCI set calculated based on Algorithm 1 is more conservative than the RCI set computed using $\bar{R}_{i+1} = D(\bar{\mathcal{R}}_i, (\mathcal{W} \times \mathcal{U}^r)) \cap \bar{R}_i$ since $\hat{D}(\bar{\mathcal{R}}_i, \rho) \subseteq D(\bar{\mathcal{R}}_i, (\mathcal{W} \times \mathcal{U}^r))$. □

Now, assuming an RCI set has been estimated, the controller synthesis task requires ensuring that the system remains within this set at all times to guarantee that the estimated end-effector position remains within the specified tolerance bound. The controller should also consider minimizing some performance objective $J(x,r,u)$ whilst retaining the system within the RCI set and obeying the system dynamic constraints. If the performance measure is to be considered over multiple steps, it is clear that the reference trajectory must be available, i.e., at $k \in \mathbb{Z}_{0+}$, $N \in \mathbb{Z}_+$ step future reference $\gamma^N_k = (r(k), \ldots, r(k+N-1))$ is assumed known. One possible choice of performance objective is $J(\cdot) = Q(y_r(k+i) - \hat{x}_{e(i|k)})^2 + Ru^2_{i|k}$, for $i \in \mathbb{Z}_{[0,N-1]}$, where Q and R are positive scalars which are used to emphasize weight on tracking performance and control effort, respectively.

As discussed previously, MPC provides a systematic way of achieving these synthesis requirements, and the resulting controller $\kappa(x(k), \gamma^N_k) := u^*_{0|k}$ results from the solution of the online optimization problem

$$\begin{aligned} U^*_k = \; & \arg\min_{U_k} \sum_{i=0}^{N-1} J\left(x_{i|k}, r_{i|k}, u_{i|k}\right) \\ \text{s.t.} \; & x_{i+1|k} = Ax_{i|k} + Bu_{i|k}, \quad r_{i|k} = r(k+i) \\ & y_r(k+i) = C_r r(k+i) \\ & x_{i|k} \in \mathcal{R}^{x,r}\left(x, r_{i|k}\right) \; \forall i \in \mathbb{Z}_{[0,N-1]} \\ & x_{0|k} = x(k) \end{aligned} \tag{20}$$

where $U^*_k = (u^*_{0|k}, \ldots, u^*_{N-1|k})$. At each time instant, the optimal control $u(k) = u^*_{0|k}$ is applied to the plant.

Remark 2: The cost function used in this article $J(\cdot) = Q(y_r(k+i) - \hat{x}_{e(i|k)})^2 + Ru^2_{i|k}$ is chosen as it aligns reasonably well with the overall control objective by penalizing tracking error and control effort. Other choices, which consider control rate or terminal costs, are possible and may result in different closed-loop responses. These alternative cost functions are not

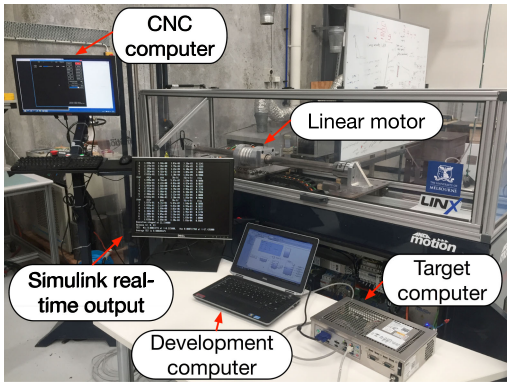

Fig. 2. Overview of experiment test bench.

investigated here but are readily accommodated in the proposed approach. Similarly, for a given R matrix, the magnitude of the elements of Q will have an effect on the closed-loop response, with larger Q typically resulting in smaller maximum tracking error at the cost of increased vibrations observed in the end effector along the reference trajectory.

Remark 3: Robustness is directly handled through the guarantees that the controller maintains the system states within the RCI set $x_{i|k} \in \mathcal{R}^{x,r}(x, r_{i|k})$. At the time of computing the RCI set, the influence of any unknown disturbance within a disturbance set $\mathcal{W}$ is considered during the iteration process. Following calculation of the RCI set, provided the feasibility of MPC is satisfied initially, the recursive feasibility of the MPC problem can be guaranteed and all state and input constraints will be satisfied in the future, i.e., robustness to any disturbance in $\mathcal{W}$ is provided.

IV. Results

A. Experimental Setup

All experiments are conducted on the test bench shown in Fig. 2. This test bench consists of a linear motor and a flexible beam, where the end effector lies at the end of the beam furthest from the motor. The LinX linear motor designed by ANCA Motion is a permanent magnet synchronous tubular motor. An aluminium flexible beam is attached on the motor base and stretches out in the direction perpendicular to the movement direction of the base. For the aluminium beam used in this experiment, the Young's modulus and density are $E = 71 \times 10^9$ N/m^2 and $\rho = 2.7 \times 10^3$ kg/m^3. The beam comes with a rectangular cross section with width $l_w = 40$ mm and thickness $l_t = 4$ mm. The characteristics of the beam and end-effector bracket are carefully designed to make the dominant resonant frequency lie within the closed-loop bandwidth of the cascaded controller.

To validate the tracking performance quantitatively, another linear encoder is installed to measure the end-effector position. The measured end-effector position is not used in the controller design process and is only used for documenting experiment results. This second encoder is installed on a linear slide to measure the end-effector movement parallel to the motor base. The end-effector measurement module is shown in Fig. 3.

B. System Identification

The disturbance F_{d1} in (1) may include friction, cogging force, and measurement noise. In this article, the friction and cogging force are identified using the procedure outlined in [21], which separates the identification of the friction and cogging forces using, respectively, the constant and frequency-dependent components of the applied force required to maintain a constant velocity. These models then enable high-fidelity simulation prior to experimental evaluation. On the other hand, since no explicit models exist for F_{d2}, the nominal model used in simulation is $F_{d2} = 0$. Furthermore, the system identification requires identifying the motor and end-effector mass, spring constant, and internal damping coefficient. To compute the robust control invariant set, the disturbance set is identified as well.

1) Step 1 Identify Cogging Force: The model of cogging force is adopted from [24]

$$F_c(x_m) = \sum_{j=1}^{P} \left(S_{cj} \sin\left(\frac{2\pi j}{\tau} x_m\right) + C_{cj} \cos\left(\frac{2\pi j}{\tau} x_m\right) \right) \tag{21}$$

where P is a positive integer number, S_{cj} and C_{cj} are the coefficients before trigonometric functions. The reference velocity is set to a small positive value, and the input force is measured. A fast Fourier transform of the measured force is then used to identify the frequency components of the cogging force, and subsequently, can be correlated to the pole pitch and further used to identify the number of harmonics P required for (21). Using this technique, the pole pitch is identified as $\tau = 87.5$ mm based on the fundamental peak, and three harmonics are required to approximate the cogging force. Subsequently, the time series data of applied force can be used to identify the remaining model parameters of cogging force using a least-squares approach, yielding $S_{c1} = 4.07$, $C_{c1} = 9.20$, $S_{c2} = 0.95$, $C_{c2} = -0.26$, $S_{c3} = -0.72$, $C_{c3} = 0.57$.

2) Step 2 Identify Friction Force: The friction model employed in simulations is based on the Lorentzian model of [25] employing the Karnopp remedy [26] to avoid simulation issues around zero velocity

$$F_f(x_m, v_m, u) = \begin{cases} \left(f_c + b_v|v_m| + \frac{f_s}{1+\left(\frac{v_m}{v_s}\right)^2}\right) \operatorname{sgn}(v_m) & |v_m| > \lambda \\ F_e & |v_m| \le \lambda \\ & |F_e| \le |f_c + f_s| \\ (f_s + f_c)\operatorname{sgn}(F_e) & \text{otherwise} \end{cases} \tag{22}$$

where $\operatorname{sgn}(\cdot)$ is the sign function; $F_e \triangleq (k_t u - F_c(x_m))$ is the externally imposed force. The system is run at different constant speeds and the constant offset in the applied force is correlated with the friction at that speed. A least-squares method is then used to identify the parameters of (22) from the data across the speed range. For the test bench, this led to identified values of $f_c = 36.36$ N, $b_v = 250.9$ Ns/m, $f_s = 22.04$ N, $v_s = 2.82$ m/s, and $\lambda = 10^{-6}$ m/s.

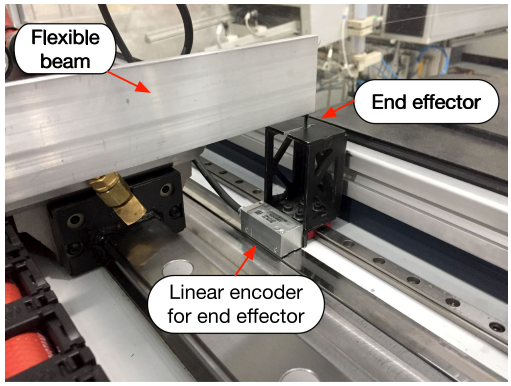

Fig. 3. End-effector measurement of experiment test bench.

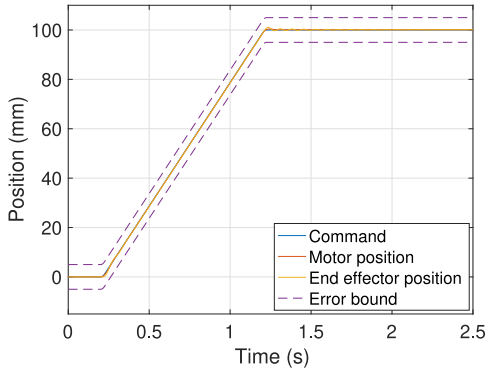

Fig. 4. Trajectory of simulated point-to-point tracking of proposed controller with $Q = 1, R = 5 \times 10^{-5}$.

3) Step 3 Identify Mechanical Subsystem Parameters: To identify the system parameters in (1), the motor runs at a constant acceleration, with the applied force measured and the disturbance force calculated from the model identified in Steps 1 and 2 above. The total effective mass of motor and end effector is subsequently identified as $M_e + M_m = 40$ kg, which is used to set a range of allowable solutions for each parameter.

A constrained optimization routine is then run to identify the values of M_m, M_e, k_s, and c_s that minimize the difference between the transient simulated end-effector trajectory and the trajectory collected from a point-to-point movement on the test bench. The outcome of this optimization was $M_e = 0.38$ kg and $M_m = 39.62$ kg, while the spring constant and damping coefficient were identified as $k_s = 2908$ N/m and $c_s = 2.10$ Ns/m.

4) Step 4 Identify Disturbance Set: To identify the lumped disturbance set $\mathcal{W}$ used in (12), a library of representative tracking trajectories is first defined. The difference between the measured and modeled motor velocities is then collected over the complete set of trajectories, leading to the population of the disturbance set. To allow for potentially unconsidered references being used, the size of the set is increased by a safety factor of 25%. For the plant of interest and its identified model, this led to a disturbance range of $\bar{w} \in [-5, 5]$ mm/s for $w \triangleq [0, \bar{w}]^T$.

C. Simulation Results and Comparison

In this section, we desire the end effector to track a reference trajectory with a tracking error bound $\epsilon = 5$ mm. The reference trajectory is described as $r \triangleq (y_r, v_r)$, where y_r and v_r are the desired position and velocity of the end effector. The reference is generated from a double-integrator model while considering position and velocity constraints, i.e., $(0, -0.1) \leq r(t) \leq (0.1, 0.1)$ [m, m/s]. Acceleration is the input to the model u_r and is subject to the constraint $-4 \leq u_r(t) \leq 4$ [m/s^2]. The LTI model of the reference (5), prior to constraint consideration, is given as follows:

$$r^+ = \begin{bmatrix} 1 & T_s \\ 0 & 1 \end{bmatrix} r + \begin{bmatrix} 0 \\ T_s \end{bmatrix} u_r \quad y_r = \begin{bmatrix} 1 & 0 \end{bmatrix} r. \tag{23}$$

The state and input constraints of the system are

$$-[5,\ 10,\ 5,\ 10]^T \leq (\xi_m, \hat{\xi}_e) \times 10^2 \leq [15,\ 10,\ 15,\ 10]^T$$
$$-9 \leq u \leq 9.$$

Yalmip [27] and MPT3 [28] are used to estimate the preset, $\hat{D}(\cdot)$ in (16). The RCI set is subsequently calculated using Algorithm 1, with the tracking error bound considered to be $\|y_r - \hat{x}_e\|_\infty \leq \epsilon_c = 4.5$ mm considering that the upper bound of the estimation error is identified as $\epsilon_o = 0.5$ mm.

1) Proposed Controller Versus Standard MPC: With the RCI set established, the proposed MPC problem can now be explicitly formulated. The cost function solved at each time step (20) uses $J = (y_r(k+i) - \hat{x}_{e(i|k)})^2 + 5 \times 10^{-5} u_{i|k}^2$ to emphasize tracking accuracy over control effort.

Fig. 4 illustrates the simulated tracking performance of the proposed controller following a point-to-point movement reference with 4 m/s^2 maximum acceleration and 0.2 s zero position waiting time. It shows that the end-effector position stays inside the error bound during the whole process.

As an initial comparison, we consider a standard tracking MPC with terminal [29] where the controller solves the following optimization at each sampling instant:

$$U^*_{\text{mpc}} = \arg\min_{U_{\text{mpc}}} \sum_{i=0}^{N-1} \left(\|y_{i|k} - y^*(k+i)\|^2_{Q1} + R_1 u^2_{i|k} \right) + \|y_{N|k} - y^*(k+N)\|^2_{P1}$$
$$\text{s.t. } x_{i+1|k} = Ax_{i|k} + Bu_{i|k} \quad y_{i|k} = Cx_{i|k}$$
$$u_{i|k} \in \mathcal{U},\ i \in \mathbb{Z}_{[0,N-1]} \quad y_{i|k} \in \mathcal{X},\ i \in \mathbb{Z}_{[1,N]}$$
$$x_{0|k} = x(k).$$

Here, $\|x\|^2_Q = x^T Q x$ and $y^* \triangleq (r, r)$ is the full state reference. The first element of U^*_{mpc} is applied to the plant. For fair comparison, the tuning weights of standard MPC are chosen as $Q_1 = \text{diag}(0, 0, 1, 0)$, $R_1 = 5 \times 10^{-5}$, and P_1 solved to discrete-time algebraic Riccati equation.

The tracking error of the proposed controller and standard MPC are illustrated in Fig. 5. It can be seen that the tracking error of standard MPC violates the 5 mm error constraint, primarily

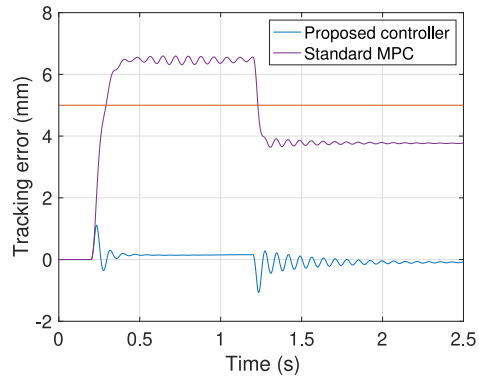

Fig. 5. Simulated end-effector tracking error by using proposed controller and standard MPC.

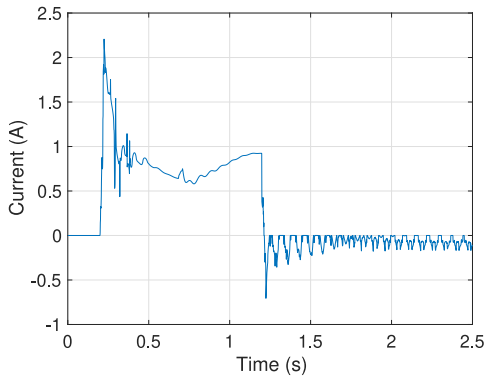

Fig. 7. Current command of proposed controller with $Q = 10^5$, $R = 0.4$ in the simulated point-to-point movement.

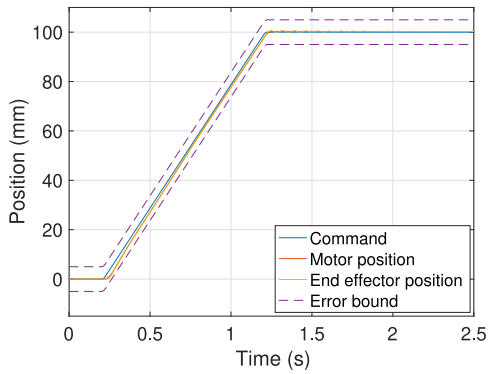

Fig. 6. Trajectory of simulated point-to-point tracking of proposed controller with $Q = 10^5, R = 0.4$.

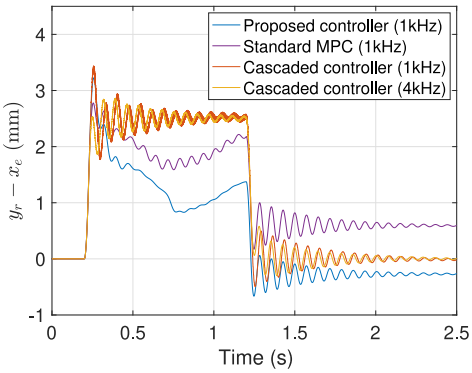

Fig. 8. Simulated end-effector tracking error by using different control methods and sampling rate for point-to-point movement.

due to the control-oriented model not capturing all dynamics. Retuning the standard tracking controller may lead to constraint satisfaction on this particular reference but is not guaranteed for other references. On the other hand, the proposed method uses the same control-oriented model but *guarantees* constraint satisfaction in the presence of the same unmodeled dynamics for all references used in the RCI set calculation.

2) Proposed Controller Versus Standard MPC and Cascaded PI Controller: Based on the fact that the cascaded PI controller is still widely used in industry, it represents a good candidate to provide a benchmark for assessing the performance of the proposed algorithm. To further demonstrate the effectiveness of the proposed controller while comparing with the cascaded controller, we retune the cost function of the proposed controller to $J = 10^5(y_r(k+i) - \hat{x}_{e(i|k)})^2 + 0.4u_{i|k}^2$ for less aggressive control. Fig. 6 illustrates the simulated tracking performance of the proposed controller resulting from the current applied as shown in Fig. 7. The end-effector position still remains inside the error bound and input current stays within the acceptable range and further validates the efficacy of the proposed approach.

Since the position of the end effector is not measurable, only the motor position and velocity errors are used by the cascaded PI architecture. This approach is typical of an industrial implementation. For a fair comparison, a notch filter was added after the calculated current command and the calibration of the cascaded controller was undertaken using the high-fidelity plant model and the same cost function used in the MPC formulation. After tuning to achieve good performance, the proportional gain and integral time constant of the velocity loop controller are $k_{pv} = 38.21$ A·s/m and $T_{iv} = 0.04$ s. The proportional gain of the position loop is chosen as $k_{pp} = 30$ 1/s. A continuous notch filter is designed with 0.80 minimum gain and 0.18 damping ratio. The continuous notch filter is then discretized by Tustin discretization and used in digital control.

To provide a fairer comparison between the cascaded PI and the proposed algorithm, two sampling rates of the PI controller are considered to allow for the increased computational demand of the optimization problem in (20). In the first case, an identical sample rate of 1 kHz is initially considered for both controllers, while a faster rate of 4 kHz is also used with the PI controller to reflect the higher computational load associated with incorporation of an MPC approach and provide a "computationally agnostic" comparison of the controller architectures. To improve the performance of the standard MPC relative to Fig. 5, it is retuned with weightings $Q_1 = \text{diag}(0, 0, 10^5, 0), R_1 = 0.4$. The terminal penalty weight P_1 is subsequently found by solving the discrete-time algebraic Riccati equation using these values.

The resulting end-effector tracking errors for all four control approaches are displayed in Fig. 8. It can be seen that the tracking error of these approaches remains within the specified

error tolerance, which is not unexpected considering that the simulation model does not explicitly consider estimation error, and thus, the disturbance forces arise from the algorithm only considering nonlinear effects considered in (21) and (22). It is interesting to note, however, that the error trajectories with the proposed controller and cascaded PI at 1-kHz sample rate are very close, 3.22 and 3.44 mm, respectively. Increasing the sample rate for the cascaded PI controller to 4 kHz leads to a slightly reduced 2.86 mm maximum tracking error. As seen in Fig. 8, the retuned standard MPC exhibits comparable performance to the proposed MPC scheme, although it must be noted that this standard approach does not guarantee constraint satisfaction and requires more calibration of the cost function weights relative to the proposed approach.

Once again, the key benefit of the model-based approach becomes clearer when looking at the transient response, where significant reductions in the vibration are achieved during the constant velocity manoeuvre from 0.2 to 1.2 s. The average tracking error achieved by the proposed controller is 0.54 mm, which is approximately 20% smaller than 0.66 and 0.65 mm achieved by cascaded controller operating at 1 and 4 kHz sampling rates.

The key effectiveness of the proposed controller is that it can *guarantee* that the desired tolerance is retained. After the reference reaches the desired position of 0.1 m, the value of control input calculated based on on-line optimization is reduced considering the error bound already within the required error bound. The negative current at the steady state intends to reduce the tracking error but this force is neutralized by the unmodeled disturbance force, which can be seen from Fig. 7. This causes the small vibration and steady-state offset (albeit within the tolerance bound) of the proposed controller after deceleration; if it was desirable to fully remove the steady-state error, this could be tackled by integrator augmentation within the MPC as discussed in [13].

D. Experiment Results and Comparison

Due to the communication limits between the target computer and drive, only the experimental tracking performances of the proposed controller and cascaded PI controller with 1-kHz sampling rate are demonstrated. The same tuning parameters and constraint tolerances as discussed in Section IV-C2 are considered here, although the optimization problem (20) and solver are matched using CVXGEN to ensure fast on-line implementation [30].

Initially, the same point-to-point reference tracking is conducted. The tracking performance and current output of the proposed controller are given in Figs. 9 and 10, respectively. As expected, the trajectory of the end effector lies inside the error bound and the state and input constraints are obeyed, which supports the proposed controller's ability to maintain error tolerances in the case of further unmodeled disturbances than were considered in the simulation.

As the end-effector position was measured (although not used in either control formulation), it is possible to present the corresponding estimated tracking error and the measured

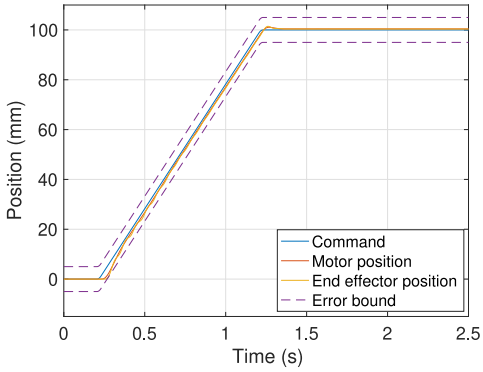

Fig. 9. Trajectory of experimental point-to-point tracking of proposed controller.

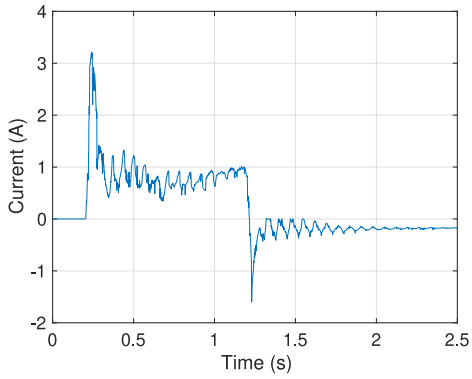

Fig. 10. Current command of proposed controller in the experimental point-to-point movement.

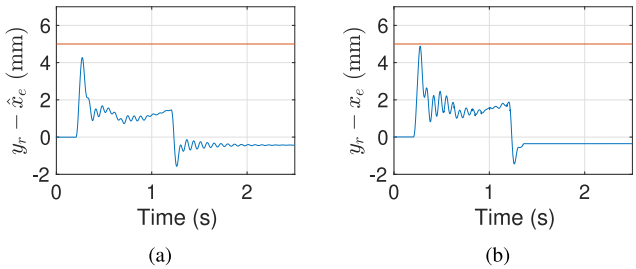

Fig. 11. Experimental end-effector tracking error of proposed controller based on point-to-point reference: (a) estimated error and (b) actual error.

tracking error, as shown in Fig. 11. The maximum estimated and actual tracking error of end effector are $\|y_r - \hat{x}_e\|_\infty = 4.27$ mm and $\|y_r - x_e\|_\infty = 4.88$ mm.

As seen from Fig. 11, the estimated tracking error is within the ϵ_c bound and the actual tracking error is within the ϵ error bound. Also, the same tracking error offset as shown in simulation can be seen at the steady state. The vibration after deceleration is smaller compared to the simulation (in this case helpful) because an unmodeled disturbance (friction) on the end effector is not considered in the simulation.

For comparison, the trajectory tracking of the same point-to-point reference based on the cascaded controller is conducted,

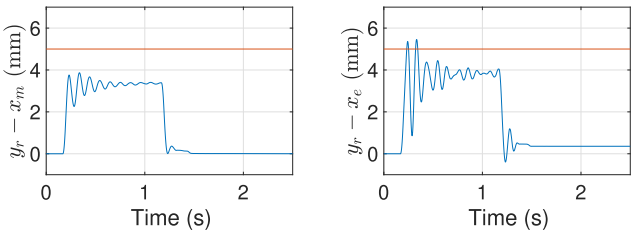

(a) (b)

Fig. 12. Experimental end-effector tracking error of cascaded PI controller based on point-to-point reference: (a) motor side and (b) end-effector side.

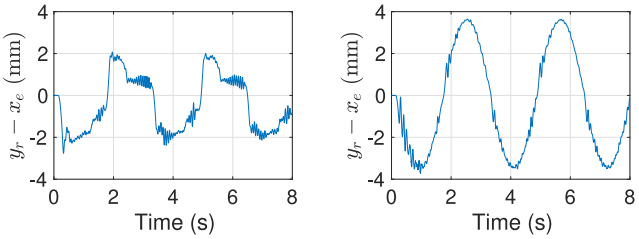

(a) (b)

Fig. 13. Experimental sinusoidal reference end-effector tracking error of two methods: (a) proposed controller and (b) cascaded PI controller.

and the tracking error is shown in Fig. 12. In this case, the maximal tracking error from the motor and end-effector side is 3.87 and 5.46 mm, respectively. It can be seen that the tracking error on the motor side is within the desired error bound. However, the end-effector tracking error exceeds the error bound, and a more obvious oscillation can be seen on the end-effector tracking error, Fig. 12(b), compared to the performance of the proposed controller, Fig. 11(b).

To further assess the capabilities of the proposed approach, a cosine reference $y_r = 0.05 + 0.05\cos(2t)$ is considered. This form of reference is typical in generating a circular contour in machining applications. The end-effector tracking error of the two control methods is presented in Fig. 13. It shows that he maximum tracking error is reduced from 3.71 to 2.76 mm using the proposed method. Although the error tolerance is achieved by the cascaded PI controller, the qualitative assessment of the two trajectories suggests that the proposed approach may be able to achieve a tighter error bound.

The experimental results demonstrate the potential for implementing the proposed control scheme on a machine with an industrial-level sampling rate. Furthermore, the proposed approach, in being able to guarantee a given tolerance, offers substantial benefit in machining applications. Naturally, while the performance of the proposed approach is superior in the case studies considered, this does come at a computational cost, as the average computation time of MPC in the experiments considered was found to be 0.69 ms at each sampling instant, which is substantially higher than that of the cascaded PI algorithm, 0.04 ms. The maximum computation time of MPC and cascaded PI is 0.72 and 0.13 ms, respectively. The relative merit of ensuring tolerance bounds met using the proposed approach must, therefore, be weighed against the potential increase in computational, and therefore, financial cost when fully considering the choice of which algorithm to use in an industrial context.

V. Conclusion

An error-bounded tracking control scheme based on an MPC structure was proposed in this article. The approach required the estimation of the maximal RCI set to ensure that feasibility and stability guarantees for the approach are possible. As existing approaches for estimating RCI sets may not converge, an augmented approach was proposed.

The proposed robust MPC algorithm was then tested in both simulation and on a linear motor test rig with a flexible connection to the end effector. It was demonstrated that the proposed controller guarantees the satisfaction of the specified end-effector error bound and can be implemented in real time on an industrial machine with a 1-ms sampling time. By contrast, the error bound was exceeded by a conventional cascaded PI controller with notch filter.

References

[1] M. Corapsiz and K. Erenturk, "Trajectory tracking control and contouring performance of three dimensional CNC," *IEEE Trans. Ind. Electron.*, vol. 63, no. 4, pp. 2212–2220, Apr. 2015.

[2] W. He and S. S. Ge, "Vibration control of a flexible beam with output constraint," *IEEE Trans. Ind. Electron.*, vol. 62, no. 8, pp. 5023–5030, Aug. 2015.

[3] L. Lu, Z. Chen, B. Yao, and Q. Wang, "A two-loop performance-oriented tip-tracking control of a linear-motor-driven flexible beam system with experiments," *IEEE Trans. Ind. Electron.*, vol. 60, no. 3, pp. 1011–1022, Mar. 2013.

[4] P. J. Serkies and K. Szabat, "Application of the MPC to the position control of the two-mass drive system," *IEEE Trans. Ind. Electron.*, vol. 60, no. 9, pp. 3679–3688, Sep. 2013.

[5] D. J. Gordon and K. Erkorkmaz, "Precision control of a T-type gantry using sensor/actuator averaging and active vibration damping," *Precis. Eng.*, vol. 36, no. 2, pp. 299–314, 2012.

[6] M. A. Stephens, C. Manzie, and M. C. Good, "On the stability analysis and modelling of a multirate control direct-drive machine tool axis subject to large changes in load dynamics," in *Proc. Amer. Control Conf.*, Jun. 2010, pp. 1550–1555.

[7] W. He, S. Zhang, and S. S. Ge, "Adaptive control of a flexible crane system with the boundary output constraint," *IEEE Trans. Ind. Electron.*, vol. 61, no. 8, pp. 4126–4133, Aug. 2014.

[8] S. Thomsen, N. Hoffmann, and F. W. Fuchs, "PI control, PI-based state space control, and model-based predictive control for drive systems with elastically coupled loads—A comparative study," *IEEE Trans. Ind. Electron.*, vol. 58, no. 8, pp. 3647–3657, Aug. 2011.

[9] A. Kamalzadeh and K. Erkorkmaz, "Compensation of axial vibrations in ball screw drives," *CIRP Ann.*, vol. 56, no. 1, pp. 373–378, 2007.

[10] T. Miyazaki, H. Kataoka, S. Tungpataratanawong, K. Ohishi, and S. Katsura, "Vibration suppression motor drive control for industrial robot using notch filter with little phase error," in *Proc. Power Convers. Conf. - Nagoya*, Apr. 2007, pp. 1618–1623.

[11] G. Zhang and J. Furusho, "Speed control of two-inertia system by PI/PID control," *IEEE Trans. Ind. Electron.*, vol. 47, no. 3, pp. 603–609, Jun. 2000.

[12] K. Szabat and T. Orlowska-Kowalska, "Vibration suppression in a two-mass drive system using PI speed controller and additional feedbacks—Comparative study," *IEEE Trans. Ind. Electron.*, vol. 54, no. 2, pp. 1193–1206, Apr. 2007.

[13] M. A. Stephens, C. Manzie, and M. C. Good, "Model predictive control for reference tracking on an industrial machine tool servo drive," *IEEE Trans. Ind. Inform.*, vol. 9, no. 2, pp. 808–816, May 2013.

[14] E. J. Fuentes, C. A. Silva, and J. I. Yuz, "Predictive speed control of a two-mass system driven by a permanent magnet synchronous motor," *IEEE Trans. Ind. Electron.*, vol. 59, no. 7, pp. 2840–2848, Jul. 2012.
[15] G. C. Chiu and M. Tomizuka, "Contouring control of machine tool feed drive systems: A task coordinate frame approach," *IEEE Trans. Control Syst. Technol.*, vol. 9, no. 1, pp. 130–139, Jan. 2001.
[16] S. Di Cairano and F. Borrelli, "Reference tracking with guaranteed error bound for constrained linear systems," *IEEE Trans. Autom. Control*, vol. 61, no. 8, pp. 2245–2250, Aug. 2016.
[17] M. Rungger and P. Tabuada, "Computing robust controlled invariant sets of linear systems," *IEEE Trans. Autom. Control*, vol. 62, no. 7, pp. 3665–3670, Jul. 2017.
[18] F. Blanchini, "Set invariance in control," *Automatica*, vol. 35, no. 11, pp. 1747–1767, 1999.
[19] S. Rakovic, E. Kerrigan, D. Mayne, and J. Lygeros, "Reachability analysis of discrete-time systems with disturbances," *IEEE Trans. Autom. Control*, vol. 51, no. 4, pp. 546–561, Apr. 2006.
[20] S. Di Cairano and F. Borrelli, "Constrained tracking with guaranteed error bounds," in *Proc. IEEE Conf. Decis. Control*, 2013, pp. 3800–3805.
[21] M. Yuan, C. Manzie, M. Good, I. Shames, F. Keynejad, and T. Robinette, "Bounded error tracking control for contouring systems with end effector measurements," in *Proc. 20th IEEE Int. Conf. Ind. Technol.*, 2019, pp. 66–71.
[22] A. Tzes and S. Yurkovich, "An adaptive input shaping control scheme for vibration suppression in slewing flexible structures," *IEEE Trans. Control Syst. Technol.*, vol. 1, no. 2, pp. 114–121, Jun. 1993.
[23] S. Rakovic, E. Kerrigan, K. Kouramas, and D. Mayne, "Invariant approximations of the minimal robust positively invariant set," *IEEE Trans. Autom. Control*, vol. 50, no. 3, pp. 406–410, Mar. 2005.
[24] C, Hu, B. Yao, and Q. Wang, "Coordinated adaptive robust contouring control of an industrial biaxial precision gantry with cogging force compensations," *IEEE Trans. Ind. Electron.*, vol. 57, no. 5, pp. 1746–1754, May 2010.
[25] D. P. Hess and A. Soom, "Friction at a lubricated line contact operating at oscillating sliding velocities," *J. Tribology*, vol. 112, no. 1, pp. 147–152, 1990.
[26] D. Karnopp, "Computer simulation of stick-slip friction in mechanical dynamic systems," *J. Dyn. Syst., Meas., Control*, vol. 107, no. 1, pp. 100–103, 1985.
[27] J. Lofberg, "YALMIP: A toolbox for modeling and optimization in MATLAB," in *Proc. IEEE Int. Conf. Robot. Autom.*, 2004, pp. 284–289.
[28] M. Herceg, M. Kvasnica, C. N. Jones, and M. Morari, "Multi-parametric toolbox 3.0," in *Proc. IEEE Eur. Control Conf.*, Jul. 2013, pp. 502–510.
[29] U. Maeder and M. Morari, "Offset-free reference tracking with model predictive control," *Automatica*, vol. 46, no. 9, pp. 1469–1476, 2010.
[30] J. Mattingley and S. Boyd, "CVXGEN: A code generator for embedded convex optimization," *Optim. Eng.*, vol. 13, no. 1, pp. 1–27, Mar. 2012.

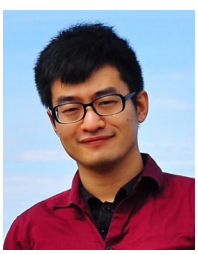

Meng Yuan (S'19) received the B.Sc. degree in automation and M.Sc. degree in control theory and control engineering from Northeastern University, Shenyang, China, in 2013 and 2015, respectively. He is currently working toward the Ph.D. degree in mechanical engineering with the University of Melbourne, Melbourne, VIC, Australia.

His research interests include the modeling and model-based control of industrial machines.

Mr. Yuan was the recipient of the Keynote Paper Award of the 25th Chinese Process Control Conference.

Chris Manzie (SM'14) received the B.S. degree in physics and the B.E.(Hons.) degree in electrical and electronic engineering from the University of Melbourne, Melbourne, Australia, both in 1996, and the Ph.D. degree in electrical and electronic engineering from the same university in 2001.

He is a Professor and the Head of the Department of Electrical and Electronic Engineering with the University of Melbourne, Melbourne, VIC, Australia, and also the Director of the cross-disciplinary Melbourne Information, Decision and Autonomous Systems (MIDAS) Laboratory. During 2003 to 2016, he was an Academic with the Department of Mechanical Engineering, with responsibilities including Assistant Dean with the portfolio of Research Training from 2011 to 2017 and Mechatronics Program Director from 2009 to 2016. He has held visiting positions with the University of California, San Diego and IFP Energies Nouvelles, Rueil Malmaison. His research interests include model-based and model-free control and optimization, with applications in a range of areas including systems related to autonomous systems, energy, transportation, and mechatronics.

Prof. Manzie is currently an Associate Editor for the IEEE TRANSACTIONS ON CONTROL SYSTEMS TECHNOLOGY and *Elsevier Mechatronics* and was an Associate Editor for *Control Engineering Practice* from 2011 to 2018 and the IEEE/ASME TRANSACTIONS ON MECHATRONICS from 2015 to 2018.

Malcolm Good (M'00) received the Ph.D. degree in mechanical engineering from the University of Melbourne, Melbourne, VIC, Australia, in 1975.

Since 1989, he has been with the Mechanical Engineering Department, University of Melbourne, serving as Head of Department from 1992 to 1996, and where he is currently an Emeritus Professor. Previously, he was Program Leader for Integrated Manufacture in the Commonwealth Scientific and Industrial Research Organisation (CSIRO) Division of Manufacturing Technology, Melbourne. He has held visiting appointments with ISVR, Southampton; HSRI, Michigan; General Electric CRD, Schenectady; and Cambridge University, Cambridge. His research has been in the fields of fluid mechanics, highway geometrics, human factors of automobile and motorcycle control, vehicular impact with roadside structures, dynamics and control of machine tools and industrial robots, and automotive drive-by-wire technologies.

Prof. Good is a Fellow of the Institution of Engineers Australia and is a member of the American Society of Mechanical Engineers and the Society of Automotive Engineers Australasia. He has been President of the Australian Robot Association, Australian Contact Person for the International Advanced Robotics Program, Interim Director of the Advanced Engineering Centre for Manufacturing, and a Program Leader and Board Member of the Research Centre for Advanced By-Wire Technologies, University of Melbourne.

Iman Shames (M'11) received the B.Sc. degree in electrical engineering from Shiraz University, Shiraz, Iran, in 2006, and the Ph.D. degree in engineering and computer science from the Australian National University, Canberra, ACT, Australia, in 2011.

He is currently an Associate Professor with the Department of Electrical and Electronic Engineering, University of Melbourne, Melbourne, VIC, Australia, where he had been a McKenzie Fellow from 2012 to 2014. Previously, he was an ACCESS Postdoctoral Researcher with the Autonomic Complex Communication Networks, Signals and Systems (ACCESS) Linnaeus Centre, Kungliga Tekniska högskolan (KTH) Royal Institute of Technology, Stockholm, Sweden. His current research interests include optimization theory and its application in control and estimation, mathematical systems theory, and security and privacy in cyber-physical systems.

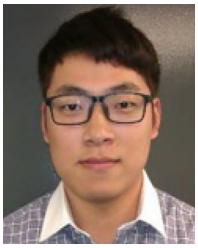

Lu Gan received the B.E. (Hons), and Ph.D. degrees in electrical engineering from RMIT University, Melbourne, Australia, in 2009 and 2014, respectively.

He joined ANCA Motion, Melbourne, Australia, initially as an Application Engineer, in 2015. Since 2017, he has been working as an Embedded Software Engineer in ANCA Motion. His current fields of study are motion control, PID auto-tuning and mechatronics control.

Farzad Keynejad received the B.Eng. degree from the Sharif University of Technology, Tehran, Iran, in 1992, and the M.Sc. degree from the Amirkabir University of Technology, Tehran, Iran, in 1995, both in mechanical engineering, and the Ph.D. degree in nonlinear optimal control from the Department of Mechanical Engineering, University of Melbourne, Melbourne, VIC, Australia, in 2009.

He is currently a Systems Engineering Technical Lead and Embedded Software Engineering Team Leader with ANCA Motion Pty. Ltd., Melbourne, VIC, Australia. His research interests include motion control systems.

Troy Robinette received the A.Dip in applied physics and computing and the B.Sc. degree in computer science from RMIT University, Melbourne, VIC, Australia, in 1994 and 1996, respectively.

From 1997 to 2001, he was with ANCA Pty. Ltd., developing and supporting software for tool and cutter grinding machines. From 2001 to 2008, he was with PBR Automotive Pty. Ltd., Melbourne, VIC, Australia were he was a Founding Member of the Brake by Wire Division responsible for all-electric park brake and electrical mechanical braking systems software development and system commissioning. From 2008 to 2014, he has been with ANCA Motion Pty. Ltd., Melbourne, VIC, Australia, where he joined as the Founding Engineering Manager to oversee the development of motion control systems for machine tools and industrial automation applications. In 2014, he transitioned to be the company's Research and Development Manager. His research interests include advanced motion control, servo drives, enhanced diagnostics, and application of Industrial Internet of Things (IIoT)/Industry 4.0.